Applied Catalysis B: Environmental 191 (2016) 42–52

Contents lists available at ScienceDirect

Applied Catalysis B: Environmental

journal homepage: www.elsevier.com/locate/apcatb

Supported TiO_2 films deposited at different energies: Implications of the surface compactness on the catalytic kinetics.

S. Rtimi [a,*], S. Giannakis [a], M. Bensimon [b], C. Pulgarin [a,*], R. Sanjines [c], J. Kiwi [a]

[a] Ecole Polytechnique Fédérale de Lausanne, EPFL-SB-ISIC-GPAO, Station 6, CH-1015, Lausanne, Switzerland
[b] Ecole Polytechnique Fédérale de Lausanne, EPFL-ENAC-GR-CEL, Station 18, CH-1015, Lausanne, Switzerland
[c] Ecole Polytechnique Fédérale de Lausanne, EPFL-SB-IPMC-JCMP, Station 3, CH-1015, Lausanne, Switzerland

ARTICLE INFO

Article history:
Received 25 December 2015
Received in revised form 3 March 2016
Accepted 9 March 2016
Available online 11 March 2016

Keywords:
TiO_2-nanoparticulate films
Adhesive sputtered films
Compactness
Antibacterial films
Photocatalysis

ABSTRACT

Insight is provided in this study for the effect of the TiO_2 film densification/compactness on polyethylene (PE-TiO_2) by sputtering TiO_2 at two very different energy levels. Uniform, adhesive low energy films were prepared by direct current magnetron sputtering (DCMS) and compared with films sputtered at high energy levels by high power impulse magnetron sputtering (HIPIMS). Nano-particulate TiO_2 films sputtered by HPIMS presented sizes of ~10.2 nm compared to films sputtered by DCMS with TiO_2 sizes of ~16.5 nm as determined by X-ray diffraction (XRD). The *E. coli* inactivation kinetics was three times faster for the samples sputtered by HIPIMS compared to their DCMS counterparts. This is an unexpected finding since the DCMS presenting larger TiO_2 sized nanoparticles released a higher amount of Ti-ions compared to the HIPIMS samples as monitored by inductively coupled plasma mass-spectrometry (ICP-MS). The Ti-ions released do not seem to react through an oligodynamic effect but diffuse through the less compact TiO_2 sputtered by DCMS. The faster bacterial inactivation kinetics observed by the HIPIMS sputtered samples can be understood in terms of the complete of Ti^{4+}/Ti^{3+} *redox* conversion during bacterial inactivation detected by X-ray photo-electron spectroscopy (XPS) compared to the smaller Ti^{4+}/Ti^{3+} effect observed in the DCMS-samples. A higher optical density was detected for the HIPIMS sputtered samples by diffuse reflectance spectroscopy (DRS). Evidence is presented for the shift in surface potential and local pH during bacterial inactivation under aerobic and anaerobic conditions. A reaction mechanism is suggested based on the findings described in this study. The sputtered films present the potential to hinder biofilm formation on flexible thin polymers/textiles widely used in hospitals and health facilities.

1. Introduction

During the last decade there has been a growing interest in the preparation of antibacterial surfaces with improved kinetics and long-term operational lifetime effective in the inactivation of all kind of pathogens, especially those where no effective antibiotics are readily available. TiO_2 composites with added bactericide metal/oxides deposited by colloids calcined on heat resistant surfaces has been the subject of many recent studies [1,2]. The effect of TiO_2-N,S nanoparticles and sputtered TiO_2 films to increase visible light absorption and accelerate bacterial inactivation kinetics have been recently reviewed by Dionysiou et al., [3,4], Foster et al., [5], Pillai et al., [6–8], Byrne et al., [9], Navabpour et al., [10], Verran et al., [11] and Bahnemann et al., [12,13]. Since the uniform and reproducible adhesion of TiO_2 films on substrates starting form colloidal depositions has been shown to present serious problems, antibacterial TiO_2 and TiO_2-composites have been recently prepared by chemical vapor deposition (CVD), by RF-sputtering and evaluated in regards to their bactericide features [14–16]. Magnetron sputtering techniques allow the deposition of uniform TiO_2 films on substrates like textiles and polymer films not able to withstand temperatures >120–150 °C [17–19].

The mechanism of *E. coli* disinfection by TiO_2 photocatalysis has been documented recently in aqueous solution [20,21] and at the solid-air interface [22,23]. Bacterial inactivation on TiO_2 films sputtered on polyester (PES) [24,25] and on polyethylene (PE) [26] presented fast bacterial inactivation kinetics in over many cycles under light irradiation. Binary oxides and Cu-decorated binary oxides of TiO_2-ZrO_2 have been investigated as TiO_2-based composites [27]. Doping TiO_2 with cations [28] and more recently with

* Corresponding authors.
E-mail addresses: sami.rtimi@epfl.ch (S. Rtimi), cesar.pulgarin@epfl.ch (C. Pulgarin).

http://dx.doi.org/10.1016/j.apcatb.2016.03.019
0926-3373/

FeOx increase the absorption of light in the visible region enhancing the bacterial inactivation under sunlight irradiation [29].

Insight is provided during this study for the different antibacterial kinetics presented by the HIPIMS TiO_2-PE samples compared to the DCMS PE-TiO_2 samples. Furthermore, this study will show that TiO_2 nano-particles present different TiO_2 planes when sputtered by HIPIMS or DCMS. The first correlation is presented between the optical film properties, surface hydrophobic-hydrophilic balance related to the amount of Ti-leached out during the bacterial inactivation as a function of the sputtered PE-TiO_2 sample. The pH changes, the OH°-radicals and the *redox* reactions on the PE-TiO_2 samples were monitored during bacterial inactivation.

The novelty of this work relates to the fact that the change in compactness and crystallographic phase of PE-TiO_2 films has been reported until now only as a function of the heating time at relatively high temperatures applied during the preparation of the TiO_2 colloids (or sol-gel) suspensions in contact with the chosen substrate [30–33]. Some studies have also report low temperature film preparation using TiO_2 colloids or pre-formed powders on PE-films by immersion, followed by drying <100 °C [34]. However, the non-uniform TiO_2 grain deposition, lack of reproducibility and adhesion makes the evaluation of the compactness estimated by surface porosity and X-ray diffraction (XRD) only qualitative. The same problems were encountered for films prepared by spray pyrolysis screen-printing [35], porous TiO_2 microstructures prepared by physical vapor deposition [36] and by the anodization of Ti-precursors in solution, addressing the preparation of films used as TiO_2 electrodes [37]. This study reports for the first time uniform, adhesive and reproducible TiO_2 films grafted on PE by sputtering with two different energies in a magnetron-sputtering chamber. This led to distinct TiO_2 particle sizes, Ti-ionic species, optical properties and crystal structures.

2. Experimental

2.1. Materials used, PE pretreatment by RF-plasma, deposition by sputtering and TiO_2-loading determination on PE

The low-density polyethylene (LDPE) consists of highly branched low crystalline semi-transparent film with the formula $H(CH_2\text{-}CH_2)_nH$. The (LDPE) 0.1 mm thick was obtained from Goodfellow, had a density of 0.92 g/cm^3, an upper temperature limit of 90 °C and a flowing point of 185 °C. The polyethylene fabrics were pretreated in the cavity of the RF-plasma unit (Harrick Corp. 13.56 MHz, 100 W) at atmospheric pressure to induce carboxylic sites able to bind TiO_2 as previously reported [26,30].

The PE was pre-treated in the cavity of the RF-plasma unit (Harrick Corp. 13.56 MHz, 100 W) at a pressure of 1 Torr. The topmost PE-layers of 2 nm (~10 atomic layers) were RF-plasma pre-treated for times between 5 min and 30 min. The O_2 in the RF- plasma cavity reacts with the PE inducing surface groups like C—O, C=O, O—C=O, C— O—O$^-$, in addition to other polar/hydrophilic groups, breaking intermolecular PE H—H bonds. These negative functionalities bind TiO_2 by electrostatics and chelation/complexation [24–28,38].

The DCMS TiO_2-samples were sputtered in O_2 atmosphere from a 5 cm diameter target (Kurt Lesker, East Sussex, UK) by direct current magnetron sputtering (DCMS) at 250 mA and 457 V (128 W). HIPMS samples were sputtered for 1–5 min applying 100 microseconds pulses each one with 350 V/5A (1750 W) with a rectangular shape operated at 100 Hz separated for 10 ms. The residual pressure P_r in the sputtering chamber was ~10^{-4} Pa. The substrate to target distance was set at 10 cm. To give an idea for the differences between DCMS and HIPIMS sputtering the main characteristics are summarized in Table 1 below.

Table 1
DCMS and HIPIMS tested sputtering parameters.

Direct current magnetron sputtering (DCMS)	High power impulse magnetron sputtering (HIPIMS)
100–300 mA	2–10 mA
100–500 V	100–500 V
Power: 5–150 W	200–500 W100–500 Hz, 0.1 ms pulse duration

The Ti-content on the polyethylene was evaluated after the Ti sputtering in reactive O_2 gas by X-ray fluorescence (XRF) in a PANalytical PW2400 spectrometer for pre-treated and non-pre-treated PE films. For non-pre-treated samples sputtered for 5 and 8 min by DCMS led to 0.031 and 0.051 TiO_2 wt%/wt PE, respectively. For samples pre-treated by RF-plasma in air for 8 min led a TiO_2 loading of 0.096 TiO_2 wt%/wt PE.

2.2. Diffuse reflectance spectroscopy (DRS), X-ray diffraction (XRD) and contact angle (CA) of TiO_2-PE deposited at different energies

Diffuse reflectance spectroscopy was carried out in a Perkin-Elmer Lambda 900 UV-VIS-NIR spectrometer provided for with a PELA-1000 accessory within the wavelength range of 200–800 nm and a resolution of 1 nm. The crystalline structure of the PE-TiO_2 film was investigated by X-ray diffraction (XRD) and recorded on an X'Pert MPD PRO from PANalytical equipped with a secondary graphite (002) monochromator and an X'Celerator detector operated in Bragg–Brentano geometry. The wettability of the PE-TiO_2 films was determined by the contact angle (CA) sessile drop method on a DataPhysics OCA 35 unit. Drop volumes of 0.5 microliter were chosen in all experiments to avoid shape alteration due to gravitational forces and to diminish the evaporation effects. The measurements were performed at room temperature (65% controlled humidity). The drop image was registered in a CCD camera (1280 × 960 pixels) attached to a microscope and processed by way of software image analysis estimating the contact angle.

2.3. E. coli inactivation on PE-TiO_2 films, stereomicroscopy, inductively plasma coupled mass-spectrometry and irradiation procedures

The samples of *Escherichia coli* (*E. coli K12* ATCC23716) on 2 cm by 2 cm PE-TiO_2 were placed into a glass Petri dish and irradiated in the cavity of a Suntest sunlight simulator (Atlas GmbH, Hanau, Germany) with a light dose of 50 mW/cm^2 emitting light in the range 310–800 nm. A cut-off filter of 400 nm was use to block the light below 400 nm (visible range). The sputtered and un-sputtered control films were kept in a sterile oven at 60 °C to avoid contamination prior to the bacterial test. The 100 μL bacteria samples were uniformly distributed on the PE-TiO_2 samples. The CFU statistical analysis of the bacteria inactivation data was performed calculating the standard deviation values. Other details of the CFU counting have been recently reported [24,27,29].

The fluorescence stereomicroscopy was carried out on samples inoculated with 10^8 CFU of *E. coli* and incubated for 2 h in a humidification chamber. This method uses a fluorochrome-based staining procedure from Filmtracer™ LIVE/DEAD® Biofilm Viability Kit (Molecular Probes, Invitrogen). The kit contains a combination of the SYTO® 9 green fluorescent nucleic acid stain and propidium iodide fluorochromes for the staining of live and dead cells, respectively. The sample fluorescence was monitored in a fluorescence stereomicroscope (Leica MZ16 FA, Leica Microsystems GmbH Wetzlar, Germany) and the images were processed using the LAS v.1.7.0 build 1240 software from Leica Microsystems CMS GmbH. Adhesion of bacteria to the sputtered polyester was allowed for 2 min

before washing the sample with sterile Milli-Q water to remove non-adherent bacteria. Images were monitored to show up both statements (live and/or dead) of bacteria on the samples.

The determination of Ti was carried out by way of a FinniganTM ICPS unit. The washing solutions from PE-TiO_2 samples were digested with nitric acid 69% (1:1HNO_3 + H_2O) to remove the organics in solution and insure that no remaining ions were kept adhered to the flask wall. The samples droplets were introduced to the ICP-MS trough a peristaltic pump to the nebulizer chamber allowing the sample components evaporation and ionization. The Ti found in the nebulizer droplets was subsequently quantified by mass spectrometry (MS).

2.4. Monitoring of the OH°-radicals by fluorescence

The quantification of the ROS (mainly OH°) was carried out based on the method proposed by Hashimoto et al., [39]. For this, an Across Chemicals 99% terephthalic acid as well as NaOH 98% from Sigma Aldrich were used. PE-TiO_2 sample of 4 cm^2 area was immersed in a 0.4 mmol L^{-1} solution of terephthalic acid dissolved in a 4 mmol L^{-1} NaOH solution. After irradiation, the solution was transferred in a quartz cell. The fluorescence of the 2-hydroxyterephthalic-acid was quantitatively monitored on a Perkin Elmer LS-50B spectrometer. The spectra were recorded between 400 and 500 nm (scan rate: 100 nm/ min) after excitation at 315 nm.

2.5. Redox couples on PE-TiO_2 films during bacterial inactivation determined by XPS

The X-ray photoelectron spectroscopy (XPS) of the PE-TiO_2 films was measured using an AXIS NOVA photoelectron spectrometer (Kratos Analytical, Manchester, UK) provided for with monochromatic AlK_a ($h\nu$ = 1486.6 eV) anode. The carbon C1s line with position at 284.6 eV was used as a reference to correct the charging effect. The surface atomic concentration was determined from peak areas using the known sensitivity factors for each element [40,41]. The spectrum background was subtracted according to Shirley [42]. The XPS spectral peaks were deconvoluted with a CasaXPS-Vision 2, Kratos Analytical UK.

3. Results and discussion

3.1. Diffuse reflectance spectroscopy (DRS), X-ray diffraction (XRD) and dynamic contact angle (CA) of PE-TiO_2 sputtered by DCMS and HIPIMS

Fig. 1 shows the optical spectra of the samples (DRS) are plotted in Kubelka-Munk (KM) unit's *vs* wavelength. The rough UV–vis reflectance cannot be plotted directly to show the optical absorption. This is due to the decrease in the transmittance introduced by the TiO_2 nano-particles. In Fig. 1, the reflectance data does not measure the PE-TiO_2 absorption coefficients because of the large scattering contribution to the reflectance spectra in Fig. 1. Fig. 1 shows the KM/S values assuming them to be proportional to the absorption of the PE-TiO_2 films within the 200–800 nm visible absorption range.

The DRS spectra of the PE-TiO_2 films shows the DCMS PE-TiO_2 absorption in Fig. 1, trace (1) plasma pretreated for 15 min and sputtered for 8 min. This spectrum is lower compared to HIPIMS sputtered samples of PE-TiO_2 plasma pretreated for 15 min and subsequently sputtered for 4 min. In both samples, the optical absorption of the TiO_2 nano-particles sets in < 400 nm as expected. Above 400 nm, the DRS spectrum of the PE-TiO_2 HIPIMS sample shows a second component, due to the HIPIMS effect on the PE-film building up n-π transitions leading to absorbing sites on the

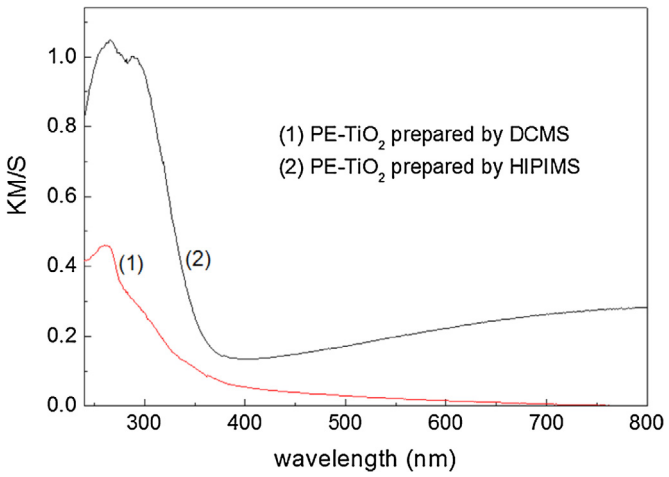

Fig. 1. Diffuse reflectance spectra of PE-TiO_2 prepared by: (1) DCMS TiO_2 sputtered for 8 min on previously pretreated-PE and (2) HIPIMS TiO_2 sputtered for 4 min on previously pretreated-PE (for more details see experimental).

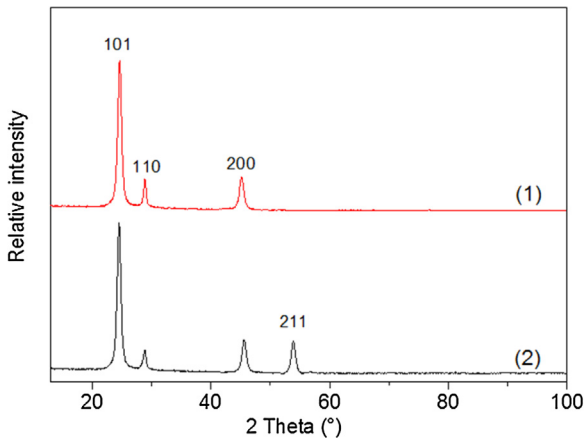

Fig. 2. XRD pattern of PE-TiO_2 films prepared via (1) DCMS and (2) HIPIMS.

PE [43]. The higher reflectance of the HIPIMS sputtered layers in Fig. 1, trace 1, provides the evidence for the dense/compact layers compared to the more transparent/porous TiO_2 layers sputtered by DCMS s shown in Fig. 1, trace 2.

Fig. 2 presents the XRD spectra of DCMS and HIPIMS PE-TiO_2 sputtered samples. The sharp narrow peaks shown in Fig. 2 indicate well-crystallized TiO_2 species. Fig. 2(1) shows the XRD patterns of the DCMS sputtered sample, all the diffraction peaks correspond to anatase phase 101,110 and 200 crystal atomic planes. Fig. 2(2) showing 4 atomic planes 101,110, 200 and 211 indicates that additional 211 atomic planes grown at the surface of PE on the HIPIMS sputtered sample. The appearance of the additional rutile 211 atomic planes was due to the higher local heat when sputtering with HIPIMS. This local heat is a consequence of the significantly higher HIPIMS power of 1750 W compared to the 450 W average power applied when sputtering by DCMS (see Experimental Section 2.1)

By inspection of Fig. 2, it is readily seen that the 101 atomic planes is the preferential growth orientation/direction in both the DCMS and the HIPIMS samples.

To estimate the crystallinity of the prepared samples, the average crystallite size was determined by the Scherrer equation: $D_{hkl} = K\lambda/(B_{hkl}\cos\theta)$, where D_{hkl} is the crystallite size in the direction perpendicular to the lattice planes, *hkl* are the Miller indices of the planes being analyzed, *K* is a numerical factor frequently referred to as the crystallite-shape factor [44], λ *is* the wavelength

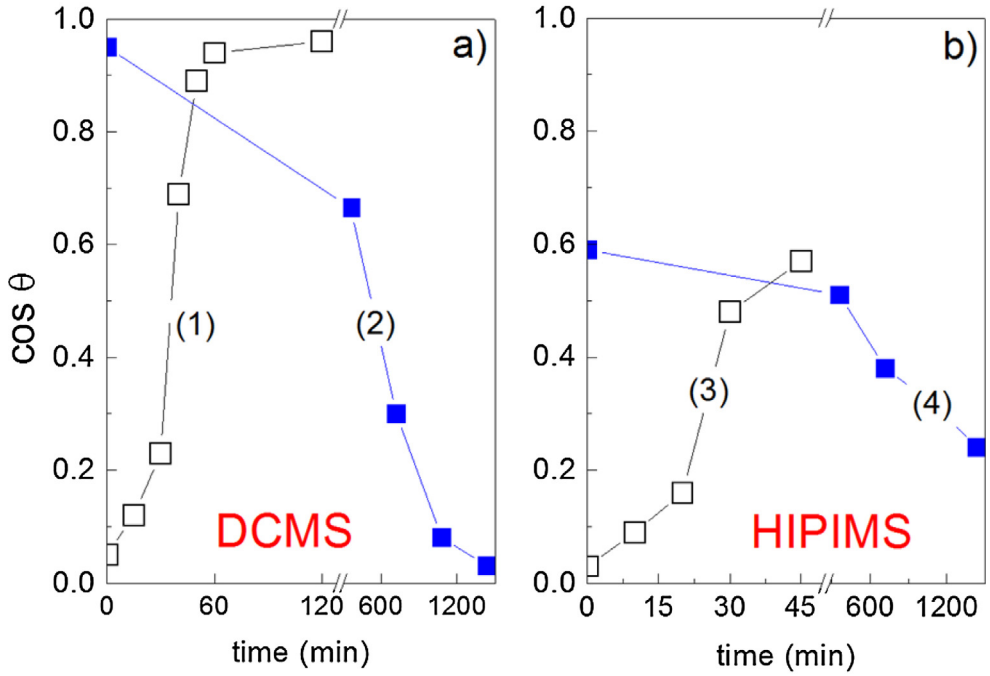

Fig. 3. Reversible photo-switchable behaviour on PE-TiO_2 samples prepared by: a) DCMS and b) HIPIMS.

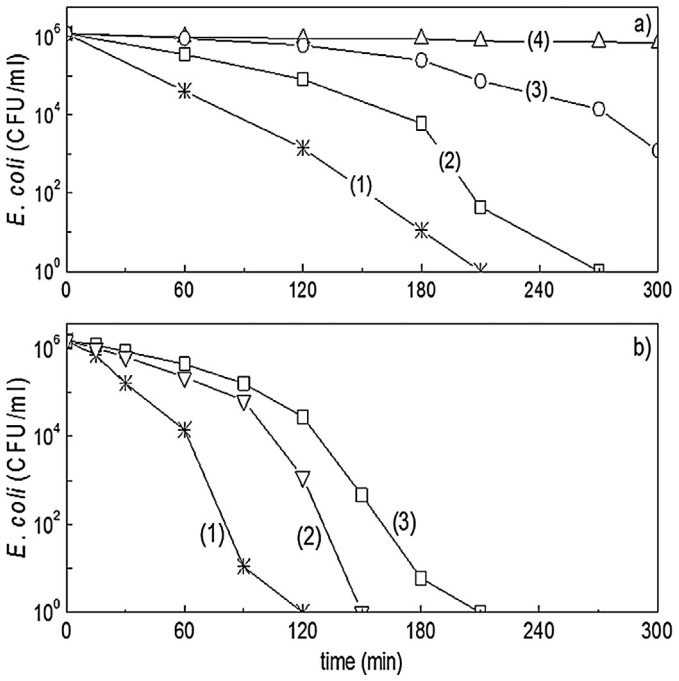

Fig. 4. (a) *E. coli* inactivation on PE-TiO_2 DCMS-sputtered for (1) 8 min, (2) 10 min, (3) 5 min and (4) PE alone under low intensity solar simulated light (50 mW/cm^2). (b) *E. coli* inactivation on PE-TiO_2 DCMS-sputtered for 8 min preceded with RF plasma surface pretreatment for: (1) 15 min, (2) 20 min and (3) 5 min under low intensity solar simulated light (50 mW/cm^2).

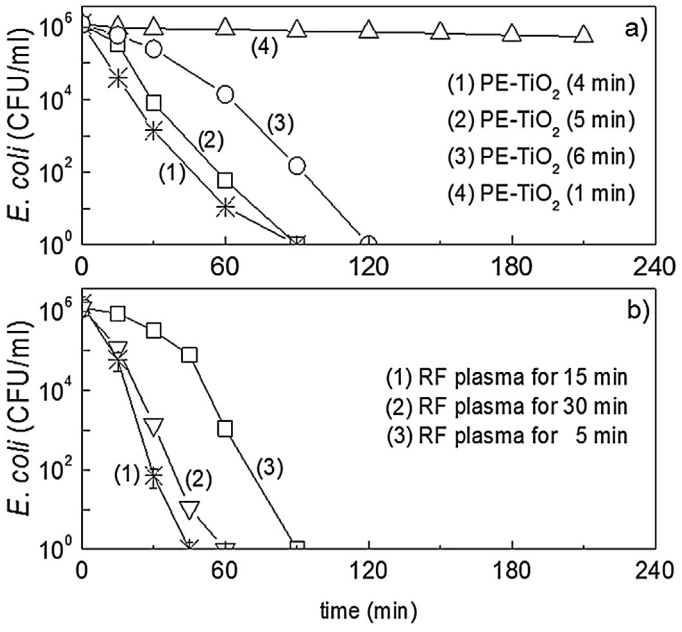

Fig. 5. (a) *E. coli* inactivation on PE-TiO_2 HIPIMS-sputtered for (1) 4 min, (2) 5 min, (3) 6 min and (4) 1 min under low intensity solar simulated light (50 mW/cm^2). (b) *E. coli* inactivation on PE-TiO_2 HIPIMS-sputtered for 4 min preceded with RF plasma surface pretreatment for: (1) 15 min, (2) 20 min and (3) 5 min.

of the X-rays, B_{hkl} is the width (full-width at half-maximum) of the X-ray diffraction peak in radians and θ s the Bragg angle. In the absence of detailed shape information of the TiO_2 crystallites as it is our case, when the Ti-atoms hit the PE, the atoms grow in different directions when sputtering by DCMS and HIPIMS and a value of $K = 0.9$ has been used as a valid approximation [45]. This leads to a grain size of PE-TiO_2 HIPIMS = 10.2 nm and a grain size of PE-TiO_2 DCMS = 16.5 nm. It is important to note that Scherrer equation is valid in the range of 100–200 nm because diffraction-peak broadening decreases with increasing crystallite size. Due to this it becomes difficult to separate the peak broadening due to crystallite size from the broadening due to other factors [45,46]. These results are in line with the results shown above in Fig. 1 by optical means. The HIPIMS nano-particles led to a DRS spectrum with a higher reflectance (see Fig. 1) compared to the DCMS spectrum, due to the increased densification due to the smaller grain size. The crystal size, atomic planes, orientation and nano-particle shape determine the TiO_2 lattice vacancies needing 1–2 eV to diffuse from the interior of the lattice to the surface [1,2,38]. Lower diffusion energies of

0.2 and 0.6 eV has been reported for the Ti^{4+}/Ti^{3+} ionic diffusion on TiO_2 crystallite surface. The ionic species associated with the HIPIMS and DCMS sputtered crystallites on PE react in a quite different form under band-gap irradiation [47,26]. Their relative relevance within the bacterial inactivation time will be further discussed in relation with the Ti-ions release.

The results for the hydrophobic to hydrophilic transformation occurring on the PE-TiO_2 sample induced by simulated solar light as reported for the first time in reference [48]. A decrease of the contact angle (CA) from 121° to less than 5° within 60 min the time of bacterial inactivation was observed (Fig. 3). A reduction of the initial contact angle (CA) to 15° within 45 min is reported for the PE-TiO_2 HIPIMS sputtered samples. During the irradiation time, the hydrophobic surface is converted to a hydrophilic surface reducing the interfacial energy between the solid and liquid surface. Fig. 3 shows the back reaction to the initial hydrophobic for PE-TiO_2 DCMS and HIPIMS sputtered samples as a function of "cos θ". According to Young's theory the "cos θ" of a liquid droplet on a solid surface is a function of the interfacial energy between the solid and the liquid [48]. The contact angle (CA) conventionally measures the angle where the liquid meets the solid quantifying the wettability of a solid surface via the Young equation. For PE-TiO_2 DCMS samples the rate of the hydrophobic to hydrophilic conversion and the rate of the reverse reaction were: 0.277 min^{-1} and 8.71×10^{-3} min^{-1} respectively. These rates were calculated according to the Young's equation [49,26]. The hydrophobic-hydrophilic equilibrium properties of the PE-TiO_2 surfaces are important in antibacterial films [5,50,26]. Recently, *E. coli* has been reported to show preferential adhesion to hydrophilic surfaces [43].

3.2. *Bacterial inactivation kinetics,* E. coli *stereomicroscopy and Ti-leaching as observed by ICP-MS during bacterial inactivation*

Fig. 4a shows the *E. coli* inactivation kinetics on DCMS PE-TiO_2 samples under light sunlight irradiation for samples sputtered by TiO_2 on PE as received (without pretreatment). Fig. 4b shows similar bacterial inactivation runs but for TiO_2 sputtered on PE RF pre-treated for different times. It is readily seen that the RF-plasma samples treated for 15 min and subsequently sputtered for 8 min in Fig. 4b, trace 1) led to the fastest bacterial inactivation (120 min). Fig. 4b, trace 2) shows a longer bacterial inactivation time for samples pre-treated for 20 min. Longer times lead to a thicker TiO_2 layers and consequently to the inward diffusion of charges [44]. This decreases the charge transfer between the PE-TiO_2 and bacteria. Fig. 4b, trace 3) shows a slow bacterial inactivation kinetics, due to the fact that when sputtering for 5 min a) did not deposit enough TiO_2 on PE or b) due to the fact that the amount of TiO_2 layers did not attain the most suitable film roughness (Rg) necessary to adhere *E. coli*. This is a preliminary step necessary for bacterial inactivation [26]. Fig. 5a presents the bacterial inactivation by HIPIMS PE-TiO_2 sputtered films without previous RF-plasma

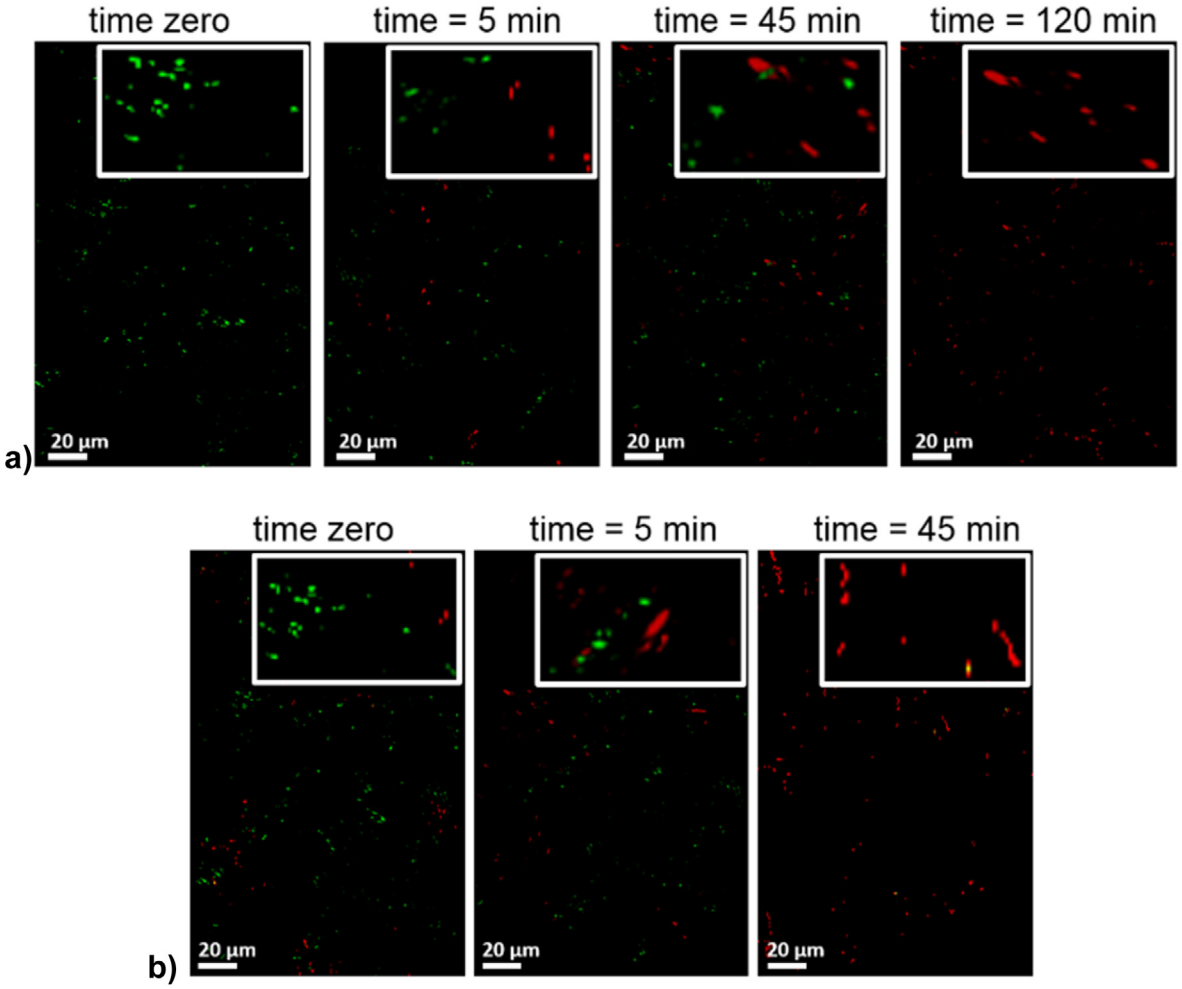

Fig. 6. Stereomicroscopy live/dead bacteria irradiated by solar simulated light at the times shown in the Figure captions on: a) PE-TiO_2 DCMS sputtered sample and b) PE-TiO_2 HIPIMS sputtered sample.

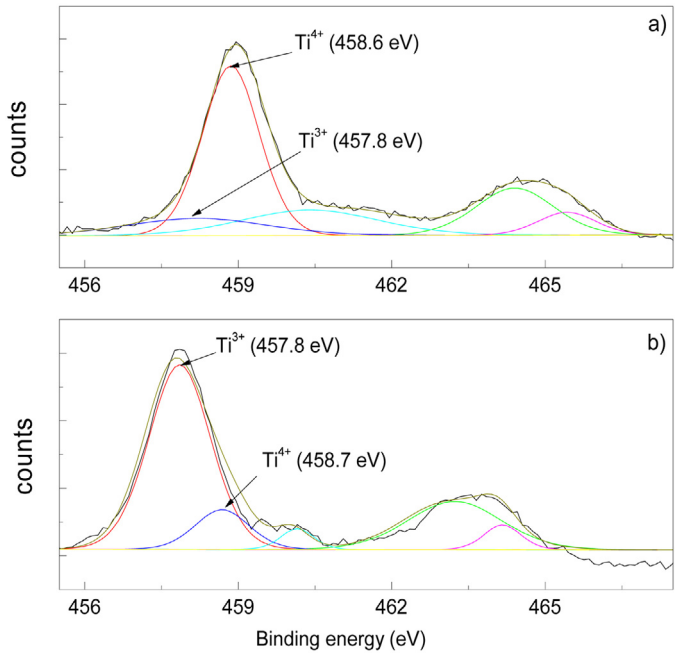

Fig. 7. Ti2p peak deconvolution of PE-TiO_2 samples RF plasma pretreated during 15 min samples and DCMS sputtered for 8 min: a) before the bacterial inactivation, and b) after bacterial inactivation under solar simulated light showing the Ti^{3+}/Ti^{4+} oxidation states variation within the bacterial inactivation period.

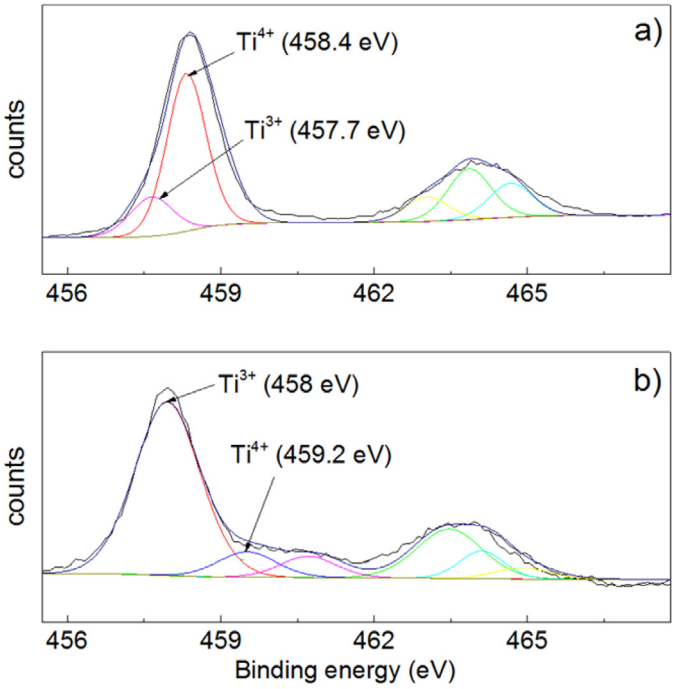

Fig. 8. Ti2p peak deconvolution of PE-TiO_2 samples RF plasma pretreated during 15 min samples and HIPIMS sputtered for 4 min: a) before the bacterial inactivation, and b) after bacterial inactivation under solar simulated light showing the Ti^{3+}/Ti^{4+} oxidation states variation within the bacterial inactivation period.

pre-treatment. Fig. 5b shows that Rf-plasma pretreatment of PE followed by 4 min HIPIMS sputtering led to the fastest inactivation time (45 min). This shows again the importance of the Rf-plasma pretreatment to induce chelating sites on the inert PE surface to graft a sufficient amount of TiO_2 layers. The bacterial inactivation kinetics in Fig. 5b, traces 2) and 3) follow a similar pattern to the one presented in Fig. 4b.

Fig. 6(a) shows the stereomicroscopy for live and dead *E. coli* bacteria by using the dye fluorochrome to stain the bacteria. For the DCMS PE-TiO_2 sputtered samples at zero time, only the green cells from the live bacteria are seen in Fig. 6a. Gradually red dots indicating membrane damage appear at times between 5 min and 45 min. Finally after 120 min only dead cell are seen in the stereomicroscopic image. This time is in agreement with the bacterial inactivation time reported by plate counting in Fig. 4b. This disappearance of all living cells in Fig. 6b coincides with the time reported in Fig. 5b for the complete bacterial inactivation evaluated by agar plate counting. Cell membrane damage is due to the increase in the outer cell membrane permeability. This leads to membrane destabilization not allowing the cell membrane to keep the osmotic pressure of the internal cytoplasm leading ultimately to cell dead [10,14,22–27]. Control experiments with *E. coli* cells incubated on PE alone kept alive up to 120 min exposure remaining green. Fig. 6b reports the data for the bacterial stereomicroscopy up to 45 min for HIPIMS sputtered samples.

3.3. XPS of PE-TiO_2 samples during bacterial inactivation and ICP-MS determination of the Ti-leached during bacterial disinfection

Redox processes on PE-TiO_2 surfaces involve Ti^{4+}/Ti^{3+} reduction occurring during the bacterial inactivation as shown in Figs. 7a,b and 8a,b. The XPS of the PE-TiO_2 DCMS sputtered samples is shown in Fig. 7a. The Ti^{4+} peak is positioned at 458.6 eV [40] before bacterial inactivation (time zero). The area of the deconvoluted [33] Ti^{4+} peak area accounts for ~95% of the total peak at time zero. Fig. 7b presents the XPS spectrogram after bacterial inactivation

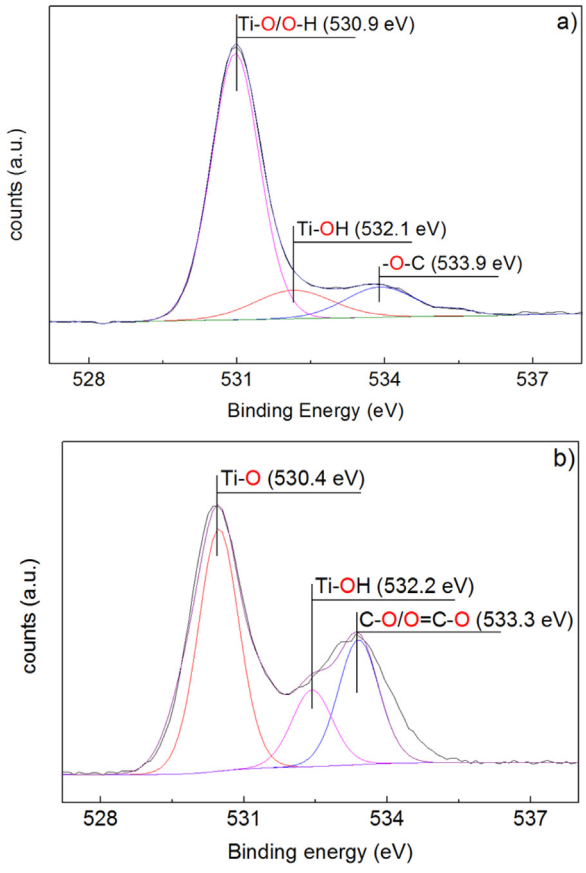

Fig. 9. O1s peak deconvolution of PE-TiO2 samples RF plasma pretreated during 15 min and DCMS sputtered for 8 min: a) before bacterial inactivation, b) after bacterial inactivation.

for this sample at 120 min. The deconvolution of the XPS peak in Fig. 7b shows that the main peak contribution at 457.8 eV is due to with Ti^{3+}. The Ti^{3+} signal amounts ~90% of the total envelope and the signal for Ti^{4+} is ~10% of the total area. The observed change in the Ti-oxidation state shows redox processes occurring at the PE-TiO_2 surface. This Ti^{4+} reduction process occurs concomitantly with the bacterial oxidation. The O-vacancies induced by DCMS and HIPIMS sputtering on TiO_2 involve the creation of unpaired electrons or Ti^{3+}-species. The reduction of Ti^{4+} occurs also in parallel with the increase in PE-TiO_2 hydrophilicity as shown in Fig. 3. The O-defect is the most important TiO_2 defect Ti-active site and its formation may be accompanied by Ti-vacancies and O-interstitial sites [1,2,17]. Defects in the TiO_2 lead to O-vacancies within the TiO_2 band-gap positioned in intermediate states (mid-gap or intra-gap states). These sates are able to trap electrons during the transition from the valence band to the conduction band [17]. The cb(e-) reacts with oxygen vacancies in the presence of O_2 leading to the O_2^- species participating in bacterial oxidation [43].

The XPS reported in Fig. 8a and b follow the pattern observed for Fig. 7a and b. The HIPIMS sputtered sample had a composition 80%Ti^{4+}: 20%Ti^{3+}. After 45 min bacterial disinfection this ratio becomes 95%Ti^{4+}: 5%Ti^{3+}. Therefore, HIPIMS sputtered samples did enhance the reduction in the initial Ti^{4+} oxidation state compared to the DCMS samples. Fig. 8b shows that in the case of HIPIMS sputtered PE-TiO_2 film, the O-vacancies found after bacterial inactivation were present in a higher amount. A concomitant creation of unpaired electrons or Ti^{3+}-species (after bacterial inactivation) was observed for the HIPIMS samples compared to the Ti^{3+} found in the DCMS samples at time zero. This is a possible reason for the faster bacterial inactivation induced by the HIPIMS samples (see Fig. 5b).

Fig. 9a shows the deconvolution for the XPS DCMS PE-TiO_2 peak before bacterial inactivation. After bacterial inactivation, Fig. 9b shows the redox process for the Ti-O species undergoing a binding energy (BE) shift from 530.9 eV to 530.4 eV. This reflects a reduction in the (O1s)-species. Concomitantly, the – C—O peak with a BE 533.9 eV shows reduction after bacterial inactivation to 533.3 eV concomitant to the bacterial oxidation. Fig. 10 reports by HIPIMS a bigger amount of XPS-counts for O1s species on the PE-TiO_2 films before and after bacterial disinfection HIPIMS compared to the counts reported for the DCMS sputtered samples in Fig. 9a and b. The shift in the XPS deconvoluted peaks reflect also the redox reactions of the surface species as shown previously for the DCMS films.

During the XPS reported in Figs. 7–10, the amount of surface oxygen vacancies responsible for the specific properties TiO_2 sputtered by HIPMS are present in a higher amount compared to the DCMS sputtered surfaces. This determines the different light absorption (DRS), XRD structure and film TiO_2 Ti^{4+}/Ti^{3+}-species as shown above by the XPS data. The higher energy applied by HIPIMS during TiO_2 and additional Ar^+ deposition (see Experimental Section) creates a considerably higher amount of O-vacancies on the TiO_2 surface compared to DCMS sputtered PE-TiO_2 [17,18,38]. The depletion of the surface lattice TiO_2 oxygen in the HIPIMS samples during bacterial inactivation leads to O-surface vacancies, but these vacancies are compensated by O_2^- due to the cb(e-) reacting with O_2 (air). One has to keep in mind that TiO_2 mediated photocatalysis is based on the fact that the adsorption of O_2 does not proceed on perfectly neutral TiO_2 surfaces, but on surfaces with excess negative charge on the surface TiO/TiOH groups as reported by XPS in Figs. 9 and 10 [17,47–49]. The O_2 adsorbed by the non-stoichiometric TiO_2 surface under light, capture cb(e-) and electrons of the O-vacancies producing superoxide/hydroperoxide radicals [1,3,26].

Fig. 11a, trace 1 and trace 2) present the Ti-ions released upon recycling by a DCMS and HIPIMS sputtered samples up to the 10th

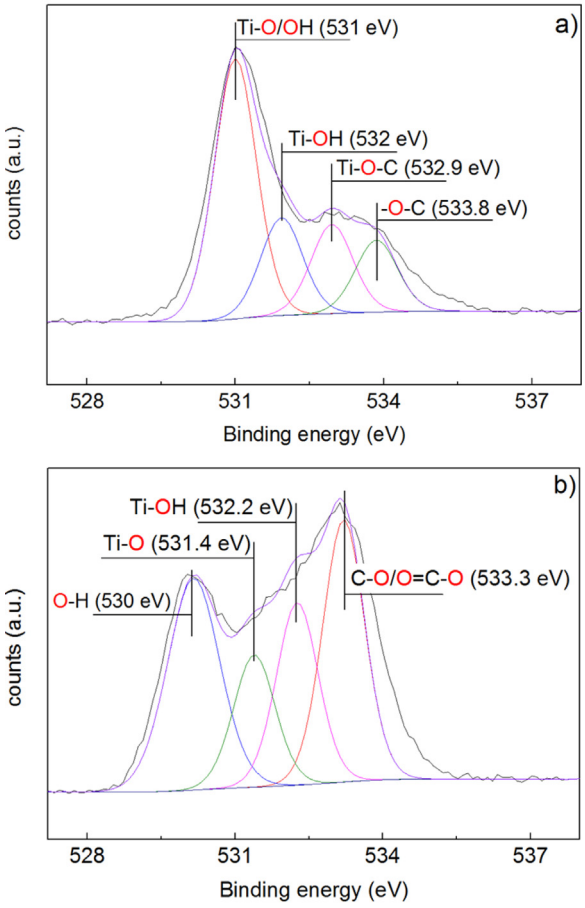

Fig. 10. O1s peak deconvolution of PE-TiO_2 samples RF plasma pretreated during 15 min and HIPIMS sputtered for 4 min: a) before bacterial inactivation, b) after bacterial inactivation.

cycle. It readily seen that no difference in the amounts of Ti were observed after the 10th recycling. However, a difference of a factor of 10 in the Ti-leaching out was observed after the first cycling of the DCMS samples due to the lower compactness of these samples (see Fig. 1) and to the DCMS samples presenting a higher resenting higher TiO_2 grain size as reported in Section 3.1. The Ti-amounts released by the DCMS compared to the HIPIMS sputtered samples are shown next in Fig. 11b and c. The trend amounts of Ti-released shown in Fig. 11b and c during repetitive bacterial inactivation cycles vary for the DCMS and the HIPIMS sputtered samples.

The ICP-MS analysis shows in Fig. 11a that the amounts of Ti-ions leached during bacterial inactivation was higher for the DCMS during the first 8 cycles compared to the HIPIMS sputtered samples. This may be the reason for the faster bacterial inactivation kinetics by the DCMS samples. Previously, Figs. 4 b and 5 b indicated that HIPIMS samples led to an inactivation about 3 times faster compared to their DCMS counterparts. This observation shows that the amount of released Ti-ions is not the main parameter controlling bacterial inactivation. Since Fig. 11 shows that more Ti is released by the samples sputtered by DCMS compared to HIPIMS sputtered samples, eliminating an oligodynamic effect due to the Ti-ions as the main cause for bacterial inactivation.

Fig. 12 shows the highly oxidative OH° radicals generated on the TiO_2 surface under band-gap irradiation leading to bacterial disinfection. Fig. 12 presents the evidence the contribution of the OH° radicals generated at the surface of the PE-TiO_2 films leading to bacterial inactivation under light irradiation. The OH° radical generation is reported as a function of time for the DCMS PE-TiO_2 sputtered samples. The increase in the fluorescence of the

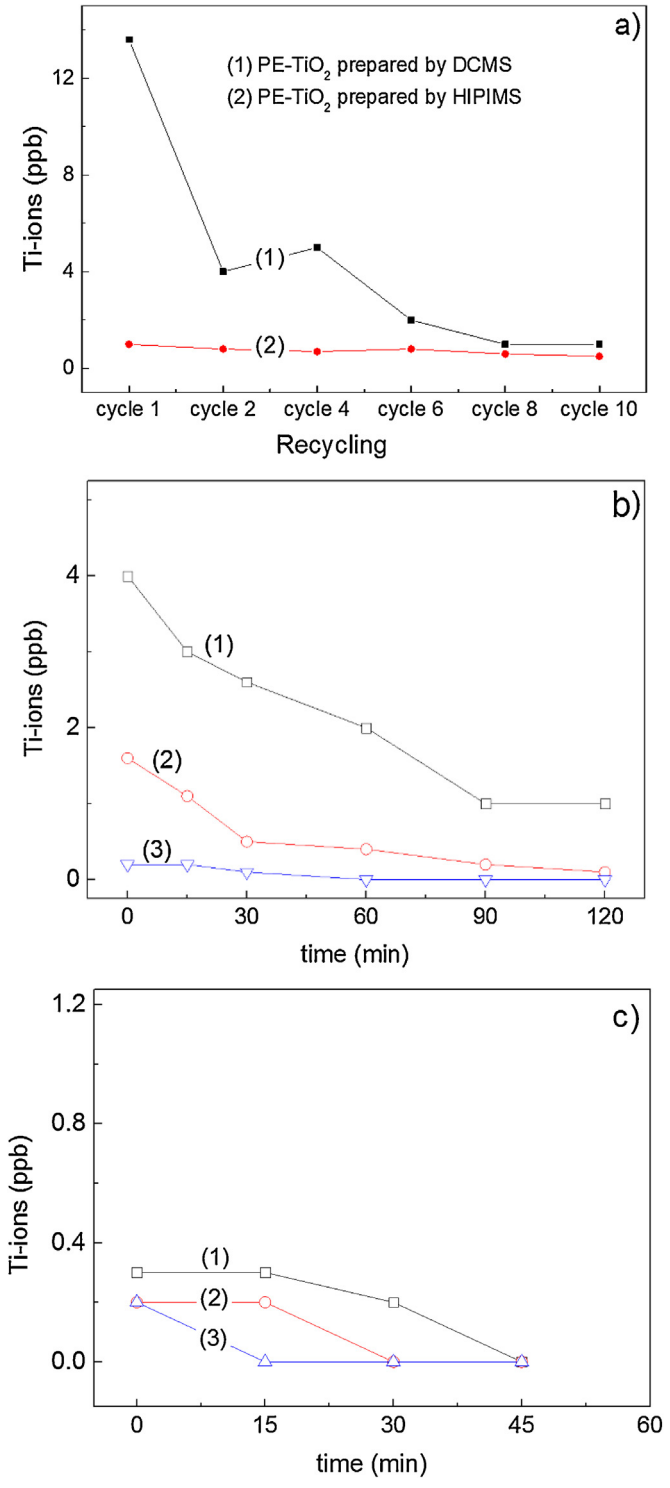

Fig. 11. (a) Ti-ions release during bacterial inactivation cycles on PE-TiO_2 prepared by: (1) DCMS (8 min sputtered; RF-plasma pretreated for 15 min) and (2) HIPIMS (4 min sputtered; RF-plasma pretreated for 15 min). (b) Ti-ions release during bacterial inactivation cycles on PE-TiO_2 DCMS samples during: (1) cycle 1, (2) cycle 2 and (3) cycle 10. (c) Ti-ions release during bacterial inactivation cycles on PE-TiO_2 HIPIMS samples during: (1) cycle 1, (2) cycle 2 and (3) cycle 10.

2-hydroxyterephthalic acid is directly proportional to the amount of OH° radical [39] and are seen to increase with irradiation time. Fig. 12, trace 1) show the OH°-generation kinetics at 26 °C and trace 2) at 50 °C. These increases reveal that the OH° generation process involves ion-molecule, radical-molecules and ion-radical species [17,38,46] since the generation of OH°-radicals alone is a process

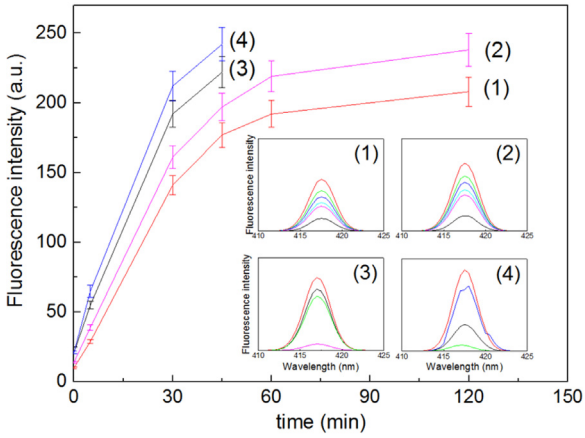

Fig. 12. OH°-radical generation as a function of the applied temperature on PE-TiO_2 samples sputtered by DCMS shown in traces 1) and 2) and HIPIMS sputtered samples shown in traces 3) and 4). The inserts 1 and 2) show the growth of the fluorescence at 25 °C and 50 °C respectively for DCMS sputtered samples. Traces 3) and 4) and inserts 3) and 4) show the growth of the fluorescence at 25 °C and 50 °C respectively for HIPIMS sputtered samples.

that does not need any activation energy. For the HIPIMS PE-TiO_2 samples, Fig. 12, traces 3) and 4) show a similar trend for the OH° radical generation as shown for DCMS samples in Fig. 11, traces 1–2).

The faster bacterial inactivation induced by the HIPIMS samples compared to the DCMS sputtered samples is shown in Scheme 1.

Scheme 1 shows the dynamic of Ti-release during *E. coli* disinfection. The DCMS less compact layers elute a large amount of Ti-ions as the number of cycles increase. The PE in the DCMS sputtering chamber was biased at a lower voltage compared to the HIPIMS biased at a much higher voltage during the TiO_2 particle deposition on PE. This has the consequence that PE binds with a much higher energy the smaller sized TiO_2 particles. This introduced a higher local compactness in the HIPIMS TiO_2 sputtered layers. The amount of TiO_2/Ti-ions released during bacterial disinfection by the DCMS and HIPIMS samples is in agreement with the results found by: a) by optical means shown in Fig. 1 by DRS b) by the particle size determined by XRD shown in Fig. 2, and c) by the redox changes in the Ti-oxidation states obtained by (XPS) in Figs. 7–10.

3.4. Main intermediates leading to bacterial inactivation

Fig. 1a, trace 1) shows the bacterial inactivation kinetics for HIPIMS TiO_2 sputtered samples in aerobic media and in anaerobic media in trace 2. The aerobic media favors the generation of highly oxidative radical intermediates. The run reported in Fig. 13a, trace 1) shows bacterial disinfection in half the time compared to the run under anaerobic conditions reported in Fig. 13a, trace 2). The Fig. 13a, trace 3) shows a more significant pH-decrease during the bacterial inactivation time in aerobic media compared to the pH-variation (Fig. 13, trace 4). The generation of HO_2°-radicals as noted in Reactions (1)–(3) below is consistent with the pH-shift shown in Fig. 13a towards more acid values during the disinfection process. Eqs.(1)–(3) outline the participation of the radicals intervening in bacterial inactivation. A complete account of the mechanism of bacterial inactivation has been reported in some recent reviews [51–55] and will not be further considered in this study. This study addresses the effect of sputtering energies on the TiO_2 films mediating bacterial inactivation and mechanistic considerations are beyond the scope of the present report.

$$TiO_2 + ligh \rightarrow TiO_2(e\text{-})cb + TiO_2(h+)vb \quad (1)$$

$$TiO_2(e^-)cb + O_2 \rightarrow O_2^- + TiO_2 \quad (2)$$

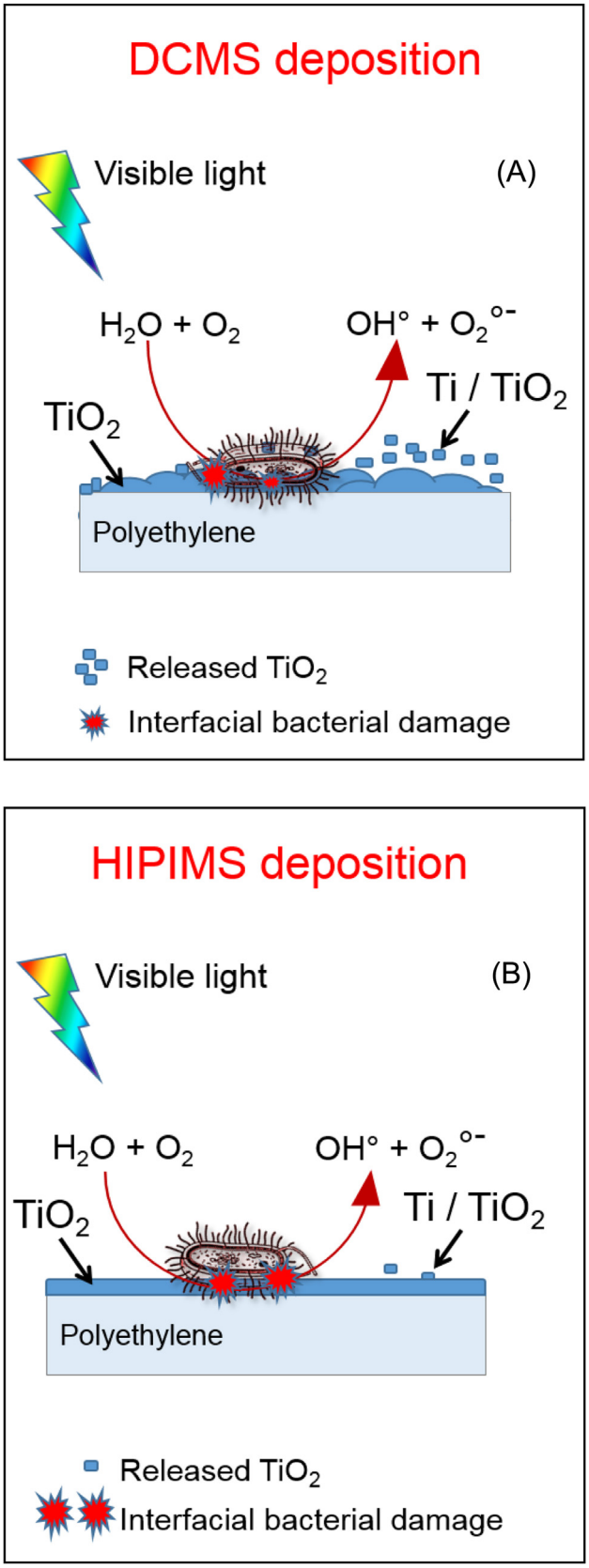

Scheme 1. Dynamics of *E. coli* disinfection on compact TiO_2 surfaces sputtered by DCMS and by HIPIMS.

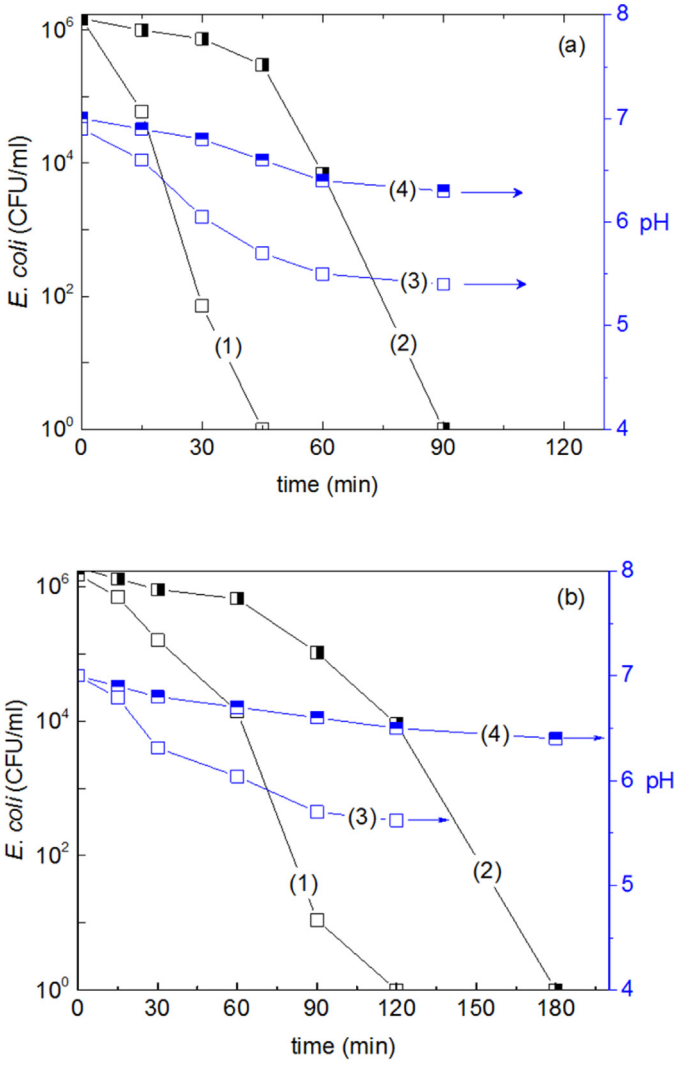

Fig. 13. (a) Bacterial inactivation on HIPIMS sputtered PE-TiO_2 related to the local-pH at the interface *E. coli* PE-TiO_2. Runs 1) and 3) were carried out under aerobic conditions and runs 2) and 4) were carried out under anaerobic conditions. (b) Bacterial inactivation on DCMS sputtered PE-TiO_2 related to the local-pH at the interface *E. coli* PE-TiO_2. Runs 1) and 3) were carried out under aerobic conditions and runs 2) and 4) were carried out under anaerobic conditions.

$$O_2^- + H_2Ov \rightarrow HO_2^\circ + H^+ + 1/2O_2 \quad (3)$$

Fig. 13b shows the bacterial inactivation runs induced by DCMS PE-TiO_2 films under sunlight irradiation. A similar trend is observed as found for Fig. 13(a) but leading to bacterial inactivation within longer times.

4. Conclusions

This study presents the first evidence by uniform, adhesive TiO_2 layers sputtered with different energies leading to PE-TiO_2 films showing different particle size, compactness, optical and redox properties. By XRD the atomic planes of HIPIMS and DCMS TiO_2-crystallites were investigated. Evidence is presented for different atomic planes in the HIPIMS PE-TiO_2 films compared with the DCMS films. By ICP-MS analysis, the amounts found for the Ti-ions leached out during disinfection were higher for the DCMS samples compared to HIPIMS samples. Bacterial inactivation was faster by a factor of about 3 on the HIPIMS samples compared to DCMS samples. The hydrophobic to hydrophilic conversion of the PE-TiO_2 surfaces under sunlight irradiation was evaluated by contact angle

(CA) and found to be similar for samples prepared by both sputtering methods as well as their photo-reversible behaviour in the dark. Local pH-changes at the TiO_2 solid-air interface were monitored during bacterial disinfection. By surface pH measurements the bacterial inactivation was shown indirectly to involve hydroperoxide (HO_2°, O_2^{-}) generated on PE-TiO_2 surface. The surface OH°-radical were monitored quantitatively as a function of time and temperature during the bacterial inactivation process. The present findings present innovative/stable PE-TiO_2 films able to inactivate bacteria within acceptable times.

Acknowledgments

We thank the EPFL and Swiss National Science Foundation (SNF) Project (200021-143283/1) for financial support. We also thank the COST Actions MP1101 and MP1106 for interactive discussions during the course of this study.

References

[1] J. Schneider, M. Matsuoka, M. Takeuchi, J. Zhang, Y. Horiuchi, M. Anpo, D. Bahnemann, Understanding TiO_2 photocatalysis: mechanism and materials, Chem. Rev. 118 (2014) 9919–9986.
[2] L. Zhang, R. Dillert, D. Bahnemann, M. Vormoor, Photo-induced hydrophilicity and self-cleaning: models and reality, En. & Environ. Sci. 5 (2012) 7491–7507.
[3] M. Pelaez, N. Nolan, S. Pillai, M. Seery, P. Falaras, A. Kontos, P.M.S. Dunlop, J. Hamilton, J.-A. Byrne, K. O'Shea, M. Entezari, D. Dionysiou, A review on the visible light active titanium dioxide photocatalysts for environmental applications, Appl. Cat. B 125 (2012) 331.
[4] S. Banerjee, C.S. Pillai, P. Falaras, K. O'shea, J.-A. Byrne, D. Dionysiou, New insights into the mechanism of visible light photocatalysis, J. Phys. Chem. Letts. 5 (2014) 2543.
[5] H. Foster, I. Ditta, S. Varghese, A. Steele, Photocatalytic disinfection using titanium dioxide: spectrum and mechanism of antimicrobial activity, Appl. Microb. & Biotech. 90 (2011) 1847.
[6] V. Etachery, G. Michlits, M.K. Seery, S.J. Hinder, S. Pillai, A highly efficient $TiO_{2-x}C_x$ nano-heterojunction photocatalyst for visible light induced antibacterial application, Appl. Mater. & Interf. 5 (2013) 1663–1672.
[7] V. Etachery, M.K. Seery, S.J. Hinder, C.S. Pillai, Oxygen rich titania, a dopant free high temperature stable and visible light active anatase photocatalyst, Adv. Functional Mater. 21 (2011) 3744–3752.
[8] V. Etachery, C. Di Valentin, J. Schneider, D. Bahnemann, C.S. Pillai, Visible-light activation of TiO_2 photocatalysts: advances in theory and experiments, J. Photochem. Photobiol. C: Photochem. Revs. 25 (2015) 1–29.
[9] J.-A. Byrne, P.S.M. Dunlop, J. Hamilton, P. Fernandez-Ibanez, I. Polo-Lopez, P. Sharma, A. Venard, A review of heterogeneous photocatalysis for water and surface disinfection, Molecules 20 (2015) 5574–5615.
[10] P. Navabpour, S. Ostovarpour, J. Hamphshire, P. Kelly, J. Verran, K. Cooke, The effect of process parameters on the structure, photocatalytic and self-cleaning properties of TiO_2 and Ag-TiO_2 coatings deposited using reactive magnetron sputtering, Thin Solid Films 571 (2014) 75–83.
[11] L. Caballero, K.A. Whitehead, N.S. Allen, J. Verran, Photocatalytic inactivation of *E. coli* using doped-TiO_2 under fluorescent irradiation, J. Photochem. Photobiol A 276 (2014) 50–57.
[12] L. Zhang, H. Mohamed, R. Dillert, D. Bahnemann, Kinetics and mechanism of charge processes in photocatalytic systems: a review, J. Photochem. Photobiol. C 13 (2012) 263–276.
[13] A. Kandiel, D. Dillert, A. Feldhoff, D. Bahnemann, Direct synthesis of photocatllytically active TiO_2 rutile nanorods partly decorated with anatase particles, J. Phys. Chem. C 114 (2010) 4909–4915.
[14] K. Page, R.G. Palgrave, I.P. Parkin, M. Wilson, P.S.L. Savin, V.A. Chadwick, Titania and silver titania composite films on glass antimicrobial coating, J. Mater. Chem. 17 (2007) 95–104.
[15] K. Page, M. Wilson, I.P. Parkin, Antimicrobial surfaces and their potential in reducing the role of inanimate environment in the incidence of hospital acquired infection, J. Mater. Chem. 19 (2009) 3819–3831.
[16] G. Walters, I.P. Parkin, The incorporation of noble metal nano-particles into host matrix films: synthesis, characterization and applications, J. Mater. Chem. 19 (2009) 574–590.
[17] A. Fujishima, X. Zhang, D. Tryck, Photocatalysis and related surface phenomena, Surf. Sci. Repts. 63 (2008) 515–582.
[18] K. Sarakinos, J. Alami, C. Konstantinidis, High power pulse magnetron sputtering: a review on the scientific and engineering state of the art, Surf. Coat. Technol. 204 (2010) 1661–1684.
[19] W. Daoud, Self-cleaning Materials and Surfaces, John Wiley and Sons Ltd., 2013.
[20] A.G. Rincon, C. Pulgarin, Photocatalytic Inactivation of *E. coli*, effect of light intensity and suspended TiO_2, Appl. Cat. B 49 (2004) 99–112.
[21] D. Gumy, C. Morais, P. Bowen, C. Pulgarin, S. Giraldo, J. Hajdu, J. Kiwi, Catalytic activity of commercial TiO_2 powders for the abatement of *E. coli*: Influence of the isoelectric point, Appl. Cat B 63 (2006) 76–84.
[22] J. Kiwi, V. Nadtochenko, New evidence for TiO_2 photocatalysis during bilayer lipid peroxidation, J. Phys. Chem. B 108 (2004) 17675–17684.
[23] R. Bacsa, J. Kiwi, T. Ohno, P. Albers, V. Nadtochenko, Preparation, testing and characterization of doped TiO_2 able to transform biomolecules under visible light irradiation by Peroxidation/Oxidation, J. Phys. Chem. B 109 (2005) 5994–6003.
[24] O. Baghriche, S. Rtimi, C. Pulgarin, T. Roussel, J. Kiwi, RF-plasma pretreatment of surfaces leading to TiO_2 coatings with improved optical absorption and OH-radical production, Appl. Cat. B 130-131 (2013) 65–72.
[25] J. Nesic, S. Rtimi, D. Laub, C. Pulgarin, G. Roglic, J. Kiwi, New evidence for TiO_2 uniform surfaces leading to complete bacterial reduction in the dark, Critical issues, Colloids Surf. B: Biointerfaces 123 (2014) 593–599.
[26] S. Rtimi, R. Sanjines, M. Andrzejczuk, C. Pulgarin, A. Kulik, J. Kiwi, Innovative transparent non-scattering TiO_2 bactericide films inducing increased *E. coli* cell fluidity, Surf. Coat. Technol. 254 (2014) 333–343.
[27] S. Rtimi, C. Pulgarin, R. Sanjines, V. Nadtochenko, J.-C. Lavanchy, J. Kiwi, Preparation and mechanism of Cu-decorated TiO_2-ZrO_2 films showing accelerated bacterial inactivation, ACS Appl. Mater. & Interf. 7 (2015) 12832–12839.
[28] J. Kiwi, C. Morrison, Heterogeneous photocatalysis: dynamics of charge transfer in Li-doped Anatase based catalysts powders with enhanced water cleavage under ultraviolet radiation, J. Phys. Chem. 88 (1984) 6146–6152.
[29] S. Rtimi, R. Sanjines, J. Kiwi, C. Pulgarin, M. Bensimon, I. Khmel, V. Nadtochenko, Innovative photocatalyst (FeOx–TiO_2): transients induced by femtosecond laser pulse leading to bacterial inactivation under visible light, RSC Adv. 5 (2015) 101751–101759.
[30] F. Gracia, J. Holgado, A. Caballero, A. Gonzales-Elipe, A. structural, optical and photo-electrochemical properties of M-TiO_2 model Film photocatalysts, J. Phys. Chem. B 108 (2004) 17466–17476.
[31] J. Liu, D. Yang, Y. Cai, Sol-Gel deposited TiO_2 Film on NiTi surgical alloys for biocompatibility improvement, Thin Solid Films 429 (2003) 225–230.
[32] X. Wang, G. Wu, B. Zhou, J. Shen, Optical constants of crystallized TiO_2 coatings prepared by sol-Gel process, Materials 6 (2013) 2819–2830.
[33] N. Avci, Ph. Smet, H. Poelman, N. Van de Velde, K. De Buysser, I. van Driessche, D. Poelman, Characterization of TiO_2 powders and thin Films prepared by non-aqueous sol-gel techniques, J. Sol-Gel Technol. 52 (2009) 424–431.
[34] Y. Zhiyong, E. Mielczarski, J. Mielczarski, D. Laub, Ph. Buffat, I. Klehm, P. Albers, K. Lee, A. Kulik, A. Renken, J. Kiwi, Preparation, stabilization and characterization of TiO_2 thin polyethylene films LDPE. photocatalytic applications, Water Res. 41 (2007) 862–874.
[35] B. Peng, G. Jungmann, C. Jager, D. Haarer, D.-W. Schmidt, M. Thelakkat, Systematic investigation of the role of compact TiO_2 layer in solid state dyes sensitized TiO_2 cells, Coord. Chem. Revs 248 (2004) 1479–1489.
[36] Y. Gaillard, V. Rico, E. Jimenes-Pique, A. Gonzales-Elipe, Nano-identification of TiO_2 thin films with different microstructures, J. Phys D: Appl. Phys. 42 (2009) 145305–145309.
[37] V. Piazza, A. Mazare, M. Diamanti, M. Pedeferri, P. Schmuki, Key oxidation parameters that influence photo-Induced properties and applications of anodic titanium oxides, J. Electrochem. Soc 163 (2016) H119–H127.
[38] C. Chan, T. Ko, N. Hiroaka, Polymer surface modification by plasma and photons, Surf. Sci. Repts. 24 (1996) 1–54.
[39] K. Ishibashi, A. Fujishima, T. Watanabe, K. Hashimoto, Detection of the active oxidative species in TiO_2 photocatalysis by using the fluorescence technique, Electrochem. Comm. 2 (2000) 207–210.
[40] Handbook of X-ray Photoelectron Spectroscopy C. D. Wanger, W. M. Riggs, L. E. Davis, J. F. Moulder and G. E.Muilenberg Perkin-Elmer Corp., Physical Electronics Division, Eden Prairie, Minnesota, USA, 1979. pp 190–195.
[41] J. Nogier, M. Delamar, P. Ruiz, P. Albers, J. Kiwi, XPS and SIMS characterization, Cat. Today 56 (2000) 403–413.
[42] D.A. Shirley, High-Resolution X-Ray photoemission spectrum of the valence bands of gold, Phys. Revs. B 5 (1972) 4709–4714.
[43] N. Turro, V. Ramamurthy, A. Scaiano, Modern molecular photochemistry of organic molecules, Univ. science Books, New York (2010).
[44] B.D. Cullity, Elements of X-ray Diffraction, 2nd Ed, Addison- Wesley, 1978.
[45] H.P. Klug, L.E. Alexander, X-Ray Diffraction Procedures, 2nd ed., Wiley, 1974, 2016 (Ch. 9).
[46] J. Winkler, Titaniun Oxide, Hannover, Vincentz, 2003.
[47] A. Nozik, Photo-electrochemistry: applications to solar energy conversion, Ann. Rev. Phys. Chem. 29 (1978) 189–192.
[48] R. Wang, K. Hashimoto, A. Fujishima, M. Chikuni, E. Kojima, A. Kitamura, M. Shimohigishi, T. Watanabe, Liquid–Induced amphiphilic surfaces, Nature 388 (1997) 431–432.
[49] N. Sakai, N. Wang, A. Fujishima, T. Watanabe, K. Hashimoto, Effect of ultrasonic treatment on highly hydrophilic TiO_2 surfaces, Langmuir 14 (1998) 5918–5920.
[50] R. Fagan, D. Mc Cormack, D. Dionysiou, S.C. Pillai, A review of solar and visible light active TiO_2 photocatalysis for treating bacteria, cyanotoxins and contaminants of emerging concern, Mat. Science Semicond. Processes 42 (2016) 2–14.
[51] J. Podporska, E. Panaitwscu, B. Quilty, L. Wang, L. Menon, S.C. Pillai, Antimicrobial properties of highly efficient photocatalytic TiO_2 nanotubes, App. Cat. B. 176-177 (2015) 70–75.

[52] A. Kubacka, M. Diez, D. Rojo, R. Bargiela, S. Ciordia, I. Zapico, J. Albar, C. Barbas, V. Martins dos Santos, M. Fernandez, Garcia M. Ferrer, Understanding the antimicrobial mechanism of TiO_2-based nanocomposite films in a pathogenic bacterium, Nature Scientific Reports 4 (2014) 4134–4143.

[53] S. pigeot-Remy, F., simonet, errazuriz-Cerda, J., lanzzaroni, D., atlan, C. guillard, photocatalysis and disinfection of water, identification of potential bacterial targets, Appl. Cat. B 104 (2011) 390–398.

[54] A. Markowska-Szczupak, K. Ulfig, A. Morawski, The Application of titanium oxide for deactivation of bio-particulates: an Overview, Cat. Today 169 (2011) 249–257.